

Scaling Q-switched microchip lasers for shortest pulses

Alex C. Butler · David J. Spence · David W. Coutts

Received: 31 May 2012/Revised: 17 August 2012
© Springer-Verlag 2012

Abstract We evaluate the design of Q-switched microchip lasers to examine the limit of their scaling to shorter picosecond pulses. A numerical model based on the laser rate equations is developed and used to predict the output characteristics of prospective laser designs. Based on the modeled results, we employ a SESAM as a passive Q-switch and thin crystals of Nd:YVO₄ as a gain medium to experimentally demonstrate the production of pulses as short as 22 ps.

1 Introduction

Applications that require sub-nanosecond pulses of light have traditionally been constrained to using mode-locked lasers. Although they can produce pulse durations from nano- to femto-seconds, mode-locked lasers are technically complex, making them expensive to purchase and maintain. To access the regime of microjoule picosecond pulses, mode-locked oscillators require pulse-picking amplification schemes that dramatically add to the size, complexity and cost of the system, often to a degree that confines them to a laboratory and is prohibitive for many applications. In particular, micro-machining, time-of-flight rangefinding and coherent anti-Stokes Raman spectroscopy (CARS) are three applications that would benefit greatly from picosecond pulses but tend to avoid mode-locked systems in favor of more accessible, if less well-suited, sources.

Q-switched lasers generally produce nanosecond pulses, but can be scaled to reach some way into the picosecond regime, to date as short as 37 ps [1]. Q-switched lasers can be more compact and less expensive than mode-locked oscillators, and typically generate higher energy pulses. Further reducing the pulse duration of Q-switched sources to compete with few-ps mode locked sources could thus greatly simplify the laser requirements for many applications.

The key to generating short pulses from Q-switched lasers is to shorten the cavity length: simple models predict that the pulse duration of a Q-switched laser, τ_p , is proportional to the resonator length with $\tau_p \approx 3.52\tau_{rt}/\Delta R$, where τ_{rt} is the cavity round-trip time and ΔR is the modulation depth of the Q-switch [1–3]. The shortest Q-switched laser pulses have been generated from microchip lasers; miniature devices that simply consist of a slab of solid-state gain material, nominally less than 2 mm thick, often with the plane-parallel resonator end mirrors coated directly onto its end faces [4–8]. This resonator design lends itself extremely well to existing wafer-like bulk manufacture methods, enabling tens, or even hundreds, of identical devices to be created from a single crystal of gain material. The resulting laser is then typically end-pumped by a laser diode source, and passively Q-switched using crystalline [7, 9–11], or semiconductor [1, 3, 12–16], saturable elements. Of these two Q-switching approaches, semiconductor saturable absorber mirrors (SESAMs) have achieved the shortest pulses by virtue of adding negligible length to the laser resonator, with generated pulses as short as 37 ps from a 185 μm resonator [1].

While shorter pulse durations would be expected from even shorter SESAM microchip lasers, current experiments have not yet remotely approached the limits of the scaling; lasers with gain crystals more than an order of magnitude shorter than demonstrated in [1] can in principle still operate

A. C. Butler (✉) · D. J. Spence · D. W. Coutts
Department of Physics and Astronomy,
MQ Photonics Research Centre, Macquarie University,
North Ryde, Sydney, NSW 2109, Australia
e-mail: alex.butler@mq.edu.au

successfully. In this paper, we examine the limits of resonator shortening for SESAM microchip lasers. By formulating a comprehensive numerical model based on the laser rate equations, we simulate SESAM-Q-switched microchip lasers, and explore the effects of length scaling on key laser characteristics such as pulse duration, repetition rate, energy and efficiency. We examine the effect of two-photon absorption in the SESAM, which becomes more significant as pulses are shortened. Finally, we use the knowledge gained from our simulations to demonstrate a record short 22 ps pulse from a 110 μm microchip laser cavity.

2 Numerical model

We first outline the development of a rate-equation model to predict the behavior of SESAM microchip lasers, which can be applied to investigate the limits to scaling-down the length of the gain element in the laser. While analytic approximations for key performance indicators have been developed [1–3], the assumptions that they contain may not be applicable in this limit. A numerical model also allows us to include the effects of nonlinear absorption in the SESAM—two-photon absorption is known to be significant [17–19], and will become increasingly important as the microchip laser is shortened to produce shorter pulses with higher intensity.

The arrangement of components in the modeled and experimental design is shown in Fig. 1. A thin laser crystal is sandwiched between a bulk output coupler and a SESAM. In this case, the SESAM has a surface coating that has high reflectivity at the pump wavelength and high transmission at the laser wavelength; this enables a double pass of the pump light through the cavity, increasing the overall absorption of the pump light. The output coupler is highly transmitting at the pump wavelength. The gain medium used in all instances is 3 % doped Nd:YVO₄, for its high gain and high absorption, which is pumped at 808 nm and emits at 1,064 nm.

A numerical model to simulate such a design was conceived based on a modified form of the laser rate equations [20], and adapted to include a time-varying loss factor that simulates a passive Q-switch as follows:

$$\begin{aligned} \frac{dn}{dt} = & -c_L \sigma_{em} n \phi \\ & + \frac{P_p}{2h\nu_p \pi r_L^2 l_L} (1 - \exp[-2(n_{tot} - n)\sigma_{abs,\pi} l_L]) \\ & + \frac{P_p}{2h\nu_p \pi r_L^2 l_L} (1 - \exp[-2(n_{tot} - n)\sigma_{abs,\sigma} l_L]) - \frac{n}{\tau_L} \end{aligned} \quad (1)$$

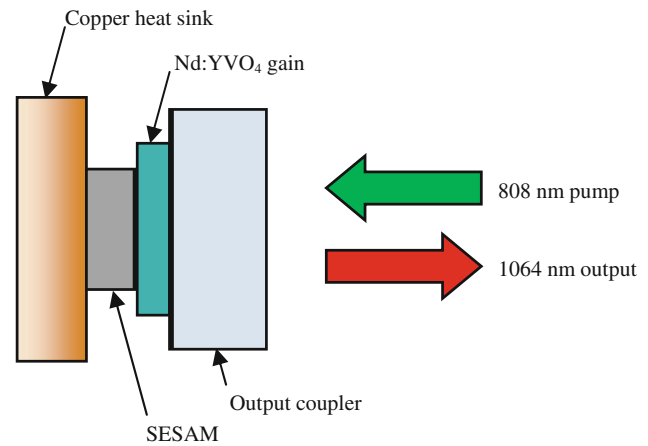


Fig. 1 A schematic of a Q-switched microchip laser, incorporating a SESAM as the passive Q-switch. The crystal-contacting face of the SESAM is coated to be highly reflective at the pump wavelength, double passing the pump beam through the cavity

$$\frac{d\phi}{dt} = c_L \sigma_{em} n \phi - \frac{-\ln[R_{OPC} R_{SESAM}(F)]}{\tau_{rt}} \phi + M \frac{n}{\tau_L} \quad (2)$$

$$\frac{dF}{dt} = c_L h\nu_L \frac{\phi}{2} - \frac{F}{\tau_{SESAM}} \quad (3)$$

$$R_{SESAM}(F) = R_U + \Delta R \left(1 - e^{-\frac{F}{F_{SAT}}}\right) \quad (4)$$

The Eqs. (1) and (2) represent the rates of change of gain inversion density, n , and cavity photon density, ϕ . The first term in each gives the rate of stimulated emission while the last term describes the rate of spontaneous emission. The spontaneous emission in (2) is required to seed the cavity mode with photons and the factor M is the coupling efficiency of fluorescence photons into the cavity mode. Since spontaneous emission is negligible compared to stimulated emission in most cases, the value of M is small and arbitrarily chosen and is non-critical in the operation of this numerical model. The remaining terms in (1) are the pumping terms: the rate of absorption of pump photons is calculated from the un-polarized incident pump power, P_p (half each for the two polarizations π and σ), the pumped volume, $\pi r_L^2 l_L$ (assuming the pump mode size is matched to the laser mode), and then scaled according to the absorptance of the gain material for π and σ polarizations. The second term in Eq. (2) expresses the round trip loss in the system, owing to the reflectivity of the output coupler, R_{OPC} , and the varying reflectivity of the SESAM, $R_{SESAM}(F)$. The quantity τ_{rt} is the photon round-trip time within the laser cavity.

Equation (3) calculates an effective photon fluence, F , incident on the face of the SESAM, taking into account the relaxation time constant, τ_{SESAM} , of the SESAM charge-carriers. Since τ_{SESAM} has duration of similar order to the

predicted laser pulse durations (the period over which the SESAM experiences a high photon flux), its inclusion in the rate equations to determine an accurate dynamic SESAM reflectivity is essential. The reflectivity of a SESAM with saturation fluence, F_{SAT} , after an incident effective photon fluence, F , is shown in (4). R_U is the unswitched reflectivity of the SESAM and ΔR the modulation depth [21]. The Nd:YVO₄ parameters used in this numerical model are given in Table 1.

A consideration for two photon absorption (TPA) in the spacer layer and Bragg mirror of the SESAM [17–19] has also been included in the numerical model. To account for this loss mechanism, we model the non-linear transmission of a zero-thickness layer on the surface of the SESAM, T_{TPA} , calculated in Eq. (5), which is dependent on the intracavity intensity incident on the SESAM, I , and a TPA parameter, β , that is fitted to measurements of the SESAM performance [21]. The modified expression for the SESAM reflectivity in Eq. (6), which replaces $R_{\text{SESAM}}(F)$ in (2), now includes a ‘roll-over term’ that decreases the SESAM reflectivity when the instantaneous intensity is high.

$$T_{\text{TPA}}(I) = \frac{1}{1 + \beta I} \quad (5)$$

$$R_{\text{SESAM,TPA}}(F, I) = R_{\text{SESAM}}(F)T_{\text{TPA}}(I) \quad (6)$$

We must make a final correction to allow for the effects of the finite thermalization rates in the upper and lower laser manifolds. This is a well-known but often neglected phenomenon [23]. Thermalization times are not well known for Nd:YVO₄, but for Nd:YAG and Nd:LSB have been measured to be of order 1 ns [23, 24]. Given that our laser pulses are $\ll 1$ ns, we can assume that during the laser pulse there is no thermalization between levels in the upper and lower manifolds: this means that only the fraction $f_a = 0.5$ of Nd³⁺ ions initially in the upper laser level (R_1 level of ⁴F_{3/2}) can contribute to stimulated transitions, and the lower laser level (Y_1 level of ⁴I_{11/2}) does not empty during the laser pulse [25]. The equations above assume rapid thermalization, where n is the population of the upper laser manifold and σ_{em} is the effective cross section. We can

heuristically alter the model by ‘turning off’ thermalization at a time t_0 approximately 1 ns before the peak of the output pulse. If the initial upper manifold population at t_0 is n_0 , we replace the stimulated emission term $c_L \sigma_{\text{em}} n \phi$ in Eqs. (1) and (2) with the new term $c_L \sigma_{\text{em}} (4n - 3n_0) \phi$. This can be derived from a treatment of the rate equations for the full set of levels [23], and one can see that as required it has the same gain at t_0 as the case with rapid thermalization, but the gain now reduces to zero when the upper laser manifold population has reduced to $3/4 n_0$, corresponding to half of the upper laser level population being transferred and accumulated in the lower laser level. The effect of the fact that the pulses are now short compared to the thermalization time is just to decrease the pulse energy by approximately a factor of $1/2 f_a \approx 0.25$, but the pulse duration is not affected since it is determined predominantly by the initial gain and the cavity lifetime [26].

The rate equations are solved numerically for sets of parameters that describe a range of potential laser designs. Due to the nature of Q-switched pulse trains (longer inter-pulse periods of steady pumping punctuated by comparatively brief and fast-changing pulses), a stiff ODE solver is used to solve the rate equations, and the evolution of n , ϕ and F (or more practically, $R_{\text{SESAM}}(F)$) during the laser action over a given period can be monitored in the solver results.

In this work, we are most interested in the laser output parameters as a function of the crystal thickness, and so we fix the other free parameters as follows: output coupler $R_{\text{opc}} = 90\%$, pump power $P_P = 200$ mW focussed to a spot of radius 9 μm .

In our experimental results in Sect. 3, we use an uncoated gain crystal that forms an air-spaced etalon with the SESAM surface. This etalon changes the effective parameters of the SESAM according to the resonance of the etalon with the cavity field; coating SESAMs with solid etalons in this way is in fact a common way to tune parameters without having to change the SESAM’s physical structure. We investigate the effect of this etalon, calculating effective values of R_U and ΔR , as well as the effective F_{SAT} and β that are altered because of

Table 1 Common constants used in Eqs. (1)–(3)

Parameter	Description	Value
c_L	Speed of light in Nd:YVO ₄ (c/n_L)	$n_L = 1.96^a$
σ_{em}	Stimulated emission cross section of Nd:YVO ₄ for π polarization	$25 \times 10^{-23} \text{ m}^2$ ^a
$\sigma_{\text{abs},\pi}$	Absorption cross section of Nd:YVO ₄ for π polarization	$1.39 \times 10^{-23} \text{ m}^2$ ^b
$\sigma_{\text{abs},\sigma}$	Absorption cross section of Nd:YVO ₄ for σ polarization	$5.46 \times 10^{-24} \text{ m}^2$ ^b
ν_P	Pump light frequency (c/λ_P)	$\lambda_P = 808 \text{ nm}$
ν_L	Laser light frequency (c/λ_L)	$\lambda_L = 1,064 \text{ nm}$
n_{tot}	Total density of Nd + ions in 3 % Nd:YVO ₄	$3.75 \times 10^{26} \text{ m}^{-3}$ ^c
τ_L	Upper state lifetime of Nd:YVO ₄	$50 \mu\text{s}^a$
M	Spontaneous photon to cavity mode coupling efficiency	$\sim 1 \times 10^{-5}$

^a From [1]

^b Measured for 808 nm pump diode with 2 nm spectral bandwidth

^c From [22]

enhancement or suppression of the field within the etalon. We present model results for a single physical SESAM: for the case of no etalon and the case of a resonant etalon, which is the typical experimental operating state of the laser. The effective SESAM parameters for these two cases are listed in Table 2.

In Fig. 2, we plot the predictions of the numerical model for the two different sets of SESAM parameters, both with and without including two photon absorption, showing the laser output characteristics as a function of cavity length.

We first consider the results in the absence of TPA. The modeling results show a linear dependence of pulse duration on cavity length, affirming that short cavities are needed to produce short pulses, with this linear relationship holding down to few-ps pulse durations. The pulse energy is almost independent of cavity length, a slightly counterintuitive feature of passively Q-switched lasers resulting from the fact that the round-trip gain at the moment of switching must be equal to unswitched cavity losses; as the cavity is shortened then the peak inversion density increases in proportion, and so the peak stored energy is independent of cavity length. The shortest possible cavity length $l_{\text{L}} = l_{\text{min}}$ is set by the limit at which a total inversion of the medium is needed to reach the gain required to switch the laser, given by setting $n = n_{\text{tot}}$ and $d\phi/dt = 0$ in Eq. (2):

$$l_{\text{min}} = \frac{-\ln(R_{\text{U}}R_{\text{OPC}})}{2\sigma_{\text{em}}n_{\text{tot}}} \quad (7)$$

For the case of no etalon and using the SESAM and output coupler parameters described above, we calculate $l_{\text{min}} = 2.6 \mu\text{m}$. The present numerical model predicts a pulse duration of just 750 fs at this cavity length, but this cavity length and pulse duration regime is outside the range of validity of the model: we do not account for the group delay associated with the penetration of the SESAM, nor the limited bandwidth of the gain material that cannot support sub-ps pulses.

Clearly the laser can Q-switch correctly using a crystal that is much thinner than the absorption length of the pump laser (192 and 488 μm for π and σ polarizations, respectively), and as such, the absorption length should not be considered a limit. The efficiency of the laser decreases

dramatically due to incomplete pump absorption; however, efficiency may not be a critical parameter to the final application, especially for cases where the pulses are to be used to seed subsequent amplifiers. As the thickness decreases, the repetition rate also decreases, partly due to the increasing inversion density required to switch, but mainly due to decreased absorption of the pump light.

The SESAM parameters have a strong influence on the output characteristics of the laser. Most important is the modulation depth ΔR , which sets the round-trip gain after switching, and is the main factor controlling the pulse energy and pulse duration. The SESAM with the resonant etalon gives more than a 20 % increase in pulse energy than the no-etalon case, and pulses shorter by more than a factor of two. However, the resonant SESAM gives a lower efficiency, mainly because of its higher effective non-saturable loss owing to the field enhancement in the etalon.

We now consider the effect of two-photon absorption on the model predictions. TPA has very little effect on pulse duration and slope efficiency, but its impression on pulse energy at short cavity lengths is appreciable. The intra-cavity intensity for short cavities is much higher than for long cavities since a similar pulse energy is delivered over a shorter time period. The effect of TPA is more severe for the resonant SESAM, since in that case the pulse energy is higher, the duration shorter, and the effective TPA coefficient is increased by field enhancement within the etalon. The main effect of TPA, an additional loss at the peak of the pulse, is to decrease the energy extracted from the inversion by each pulse. TPA does not have a strong effect on efficiency, however, as the laser produces lower energy pulses at an increased repetition rate compared to the case with no TPA. We conclude that increased TPA should not limit the generation of shorter pulses as cavities are shortened.

3 Experimental method and results

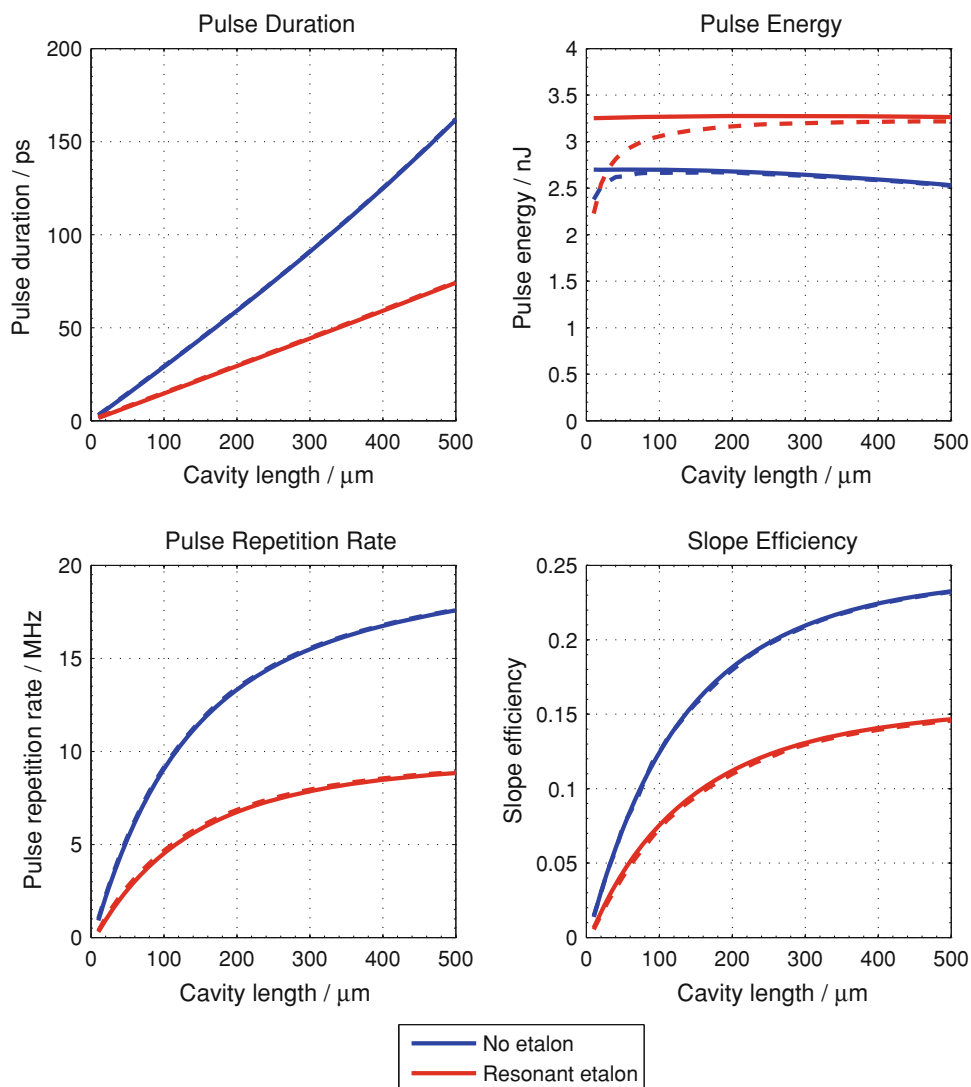
We have constructed a series of three lasers to explore the scaling of pulse duration with cavity length. The arrangement of the basic laser components is shown in Fig. 1. In all cases, the pump laser was delivered by an 808 nm diode

Table 2 Values of effective SESAM parameters used in experiment and modeling, for the case of no surface etalon, and for the resonant case

Parameter	Description	No etalon	Resonant etalon
R_{U}	Unswitched reflectivity (%)	68	47
ΔR	Modulation depth (%)	15	23
F_{SAT}	Saturation fluence ($\mu\text{J cm}^{-2}$)	70	39
β	TPA parameter ($\text{m}^2 \text{W}^{-1}$)	1×10^{-15}	1.8×10^{-15}
τ_{SESAM}	Relaxation time constant (ps)	9	

Data from BATOP GmbH (β inferred from TPA measurements)

Fig. 2 Numerical model results for a range of cavity lengths, showing operation both with and without a resonant SESAM etalon. Results that include TPA consideration are shown as dashed lines



laser through a 100 μm fiber, collimated and focused down to a spot of 10 μm radius (at e^{-2}) in the laser crystal. Since the pump diode showed better output stability at higher currents, the high-power pump beam was attenuated by an aperture placed before the collimating lens, resulting in an operating pump M^2 of 2.5.

The gain material was 3 % doped a-cut Nd:YVO₄. Since microchip lasers have thicknesses typically ≤ 2 mm and in this case ≤ 310 μm, a highly absorbing, high-gain material such as Nd:YVO₄ is ideal. The thicknesses of Nd:YVO₄ crystal tested were 310, 210 and 110 μm and the Nd:YVO₄ properties are summarized in Table 1.

The SESAM (BATOP GmbH) was mounted on a copper heat sink and had a surface coating that was highly reflecting at 808 nm and highly transmitting at 1,064 nm to allow a double pass of the cavity for the pump beam and uninterrupted access to the SESAM for the cavity field. The parameters of the SESAM under test are recorded in

Table 2. This particular SESAM was chosen for its large modulation depth (ΔR) and low saturation intensity ($F_{\text{SAT}}/\tau_{\text{SESAM}}$). The output coupler reflectivity was 90 %.

As described in Sect. 2, there was an etalon formed between the SESAM surface and the uncoated surface of the gain crystal. Effects attributed to this etalon were observed during experiments: by rastering the pump spot position across the face of the laser, we could vary the laser output behavior, specifically the pulse duration and pulse energy. The spatial dependence was caused by a small wedge in the spacing of the etalon, confirmed by observation of fringes formed between crystal and SESAM under sodium lamp illumination—the periodicity of the laser behavior across the surface was consistent with the observed fringe spacing. This wedge allowed us to access a range of effective SESAM parameters, in particular the extreme values set by the resonant etalon as shown in Table 2. We optimized the spatial location of the pump

spot to give the shortest pulse duration, as monitored using an autocorrelator. From the modeling results in Fig. 2, we deduce that the SESAM etalon is resonant with the 1,064 nm laser radiation for this optimized case. At this point we state that while operation with etalon resonance up to and including anti-resonance (defining the opposite limit to resonant operation) was observed, SESAM switching was generally unstable near anti-resonance due to the field suppression effects of the etalon. We leave further investigation of this effect to future work.

Additionally, the wedge effected a small amount of tunability on the laser output wavelength by causing a variation in the total cavity length, causing up to ± 1 nm deviation from the peak emission wavelength of 1,064.25 nm. Operation was generally on a single longitudinal mode, although in rare cases when using the 310 μm cavity, dual longitudinal mode output was observed.

The pulse duration results for these experiments are plotted in Fig. 3a and an autocorrelator trace for the shortest pulse in Fig. 3b. In Fig. 3a, we also include numerical and analytical modeling results [1–3], for the resonant SESAM etalon parameters in Table 2. Assuming a Gaussian-shaped pulse, the real pulse duration is calculated from the autocorrelator trace shown in Fig. 3b as $\tau_{\text{pulse}} = \tau_{\text{ac}}/\sqrt{2}$. The shortest pulses achieved from the 310, 210 and 110 μm cavities were 45, 33 and 22 ps, respectively. The pulse energies measured from these lasers were; 2.4, 2.8 and 0.9 nJ, compared to numerically modeled values of 3.1, 2.9 and 2.5 nJ.

In all cases the pulse trains were regular, with the repetition rate of the laser linearly dependent on pump power; for the 110 μm laser the repetition rate was selectable between 345 kHz and 2.44 MHz for pump powers in the range 50 to 100 mW. Varying the pump power was not found to have an appreciable effect on either pulse duration or energy.

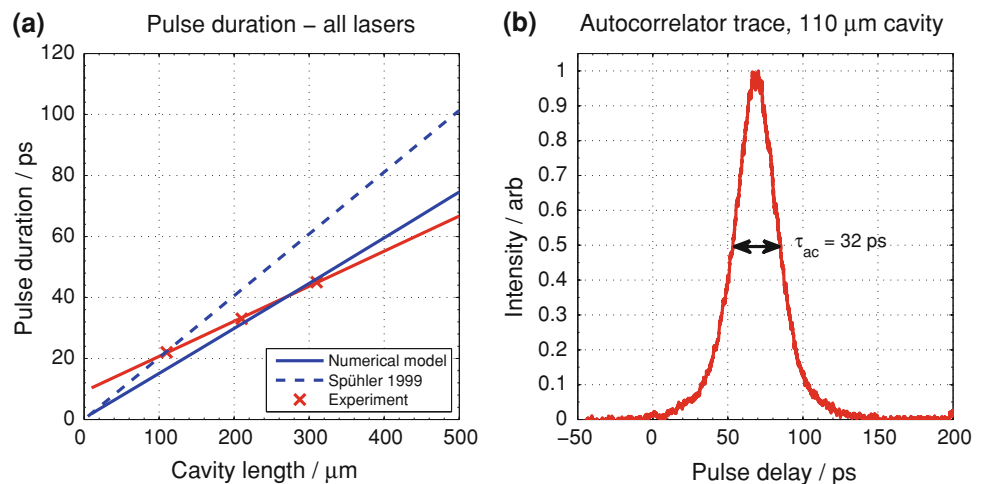
The laser mode size (radius at e^{-2}) in the crystals was measured as 8, 9 and 9 μm for the 310, 210 and 110 μm cavities, respectively (compared to a pump spot radius of 10 μm), with M^2 recorded as 1.1, 1.4 and 1.1. The laser mode size was monitored as the pump power was altered, with no discernible change.

4 Discussion

The 22 ps pulse duration measured for our 110 μm laser is currently the shortest pulse achieved from a laser of this design, compared to the previous result of Spühler et al. [1] of 37 ps. Although the length of the gain crystal is well below the absorption length for Nd:YVO₄, measured to be 192 μm for the π polarization for our 2 nm diode spectral bandwidth, we have shown that regular trains of short Q-switched pulses are practically attainable.

It is worth noting that our numerical model predictions for the SESAM operation with no etalon in Fig. 2 do not deviate significantly from the commonly used analytic models in this regime [1–3]. However, the two models diverge in cases where the saturable losses are no longer small compared to the non-saturable losses, for example when the SESAM etalon is resonant with the cavity field. Since we optimized our experimental laser for shortest pulse duration, resulting in resonant SESAM etalon operation, we find in Fig. 3a that our numerical model gives a closer fit to the experimental results than the analytic model. In pulse energy, repetition rate and slope efficiency our numerical model also gives better agreement. Other groups have reported a discrepancy between experimental results and analytically modeled predictions, for example, Spühler et al. [1] reported 37 ps, 53 nJ measured pulses, compared to 64 ps and 180 nJ predicted by their analytic

Fig. 3 **a** Pulse duration results for all lasers, including numerical and analytic predictions for a resonant SESAM etalon and **b** autocorrelator trace for the 110 μm laser



models, but our numerical model shows much closer agreement with our experimental results.

Scaling this laser design to even shorter cavity lengths should extend the observed linear trend to shorter pulse durations. Importantly, we have shown that the increasing impact of TPA in this regime should not present a barrier to reducing the pulse duration, although it will dramatically reduce pulse energy. Polishing and handling crystals of sub-100- μm thickness will require great care, although we note that beta-barium-borate crystals as thin as 10 μm are commercially available. As pulses approach the few-ps regime, additional elements of the cavity length such as air spaces between elements, and the group delay associated with reflection from the SESAM will need to be considered, along with appropriate modeling of the gain bandwidth.

5 Conclusion

A simple and compact laser that delivers pulses as short as 22 ps has been modeled and experimentally verified. Our 110 μm laser resonator was shown to reliably generate a continuous train of pulses. By sacrificing laser efficiency we have shown that a miniature Q-switched laser can deliver pulse durations comparable to larger and more complex mode-locked systems. We show that non-linear effects get more severe as pulse durations become shorter, although such effects predominantly reduce pulse energy rather than preventing the formation of short pulses. Further scaling-down of the cavity length is predicted to be beneficial and sub-10-ps pulses should be possible at the expense of laser efficiency.

In this Q-switched system a great amount of control over the low pulse repetition rate (100's of kHz compared to MHz mode-locked systems) is afforded by simply altering the pump power, or single pulses can be generated on demand by modulating the pump diode. This feature makes these Q-switched microchip lasers extremely suitable to uncomplicated, pump-scavenging amplification architectures [27], that can bring the overall system efficiency and pulse energy back up to levels of greater practical utility.

Acknowledgments A. Butler acknowledges the Macquarie University Research Excellence Scholarship, and this project was funded by a Macquarie University Research Development Grant.

References

- G.J. Spühler, R. Paschotta, R. Fluck, B. Braun, M. Moser, G. Zhang, E. Gini, U. Keller, Experimentally confirmed design guidelines for passively Q-switched microchip lasers using semiconductor saturable absorbers. *J. Opt. Soc. Am. B* **16**, 376–388 (1999)
- J.J. Zayhowski, P.L. Kelley, Optimization of Q-switched lasers. *IEEE J. Quantum Electron.* **27**, 2220–2225 (1991)
- B. Braun, F.X. Kärtner, G. Zhang, M. Moser, U. Keller, 56-ps passively Q-switched diode-pumped microchip laser. *Opt. Lett.* **22**, 381–383 (1997)
- J.J. Zayhowski, A. Mooradian, Single-frequency microchip Nd lasers. *Opt. Lett.* **14**, 24–26 (1989)
- T. Taira, A. Mukai, Y. Nozawa, T. Kobayashi, Single-mode oscillation of laser-diode-pumped Nd:YVO₄ microchip lasers. *Opt. Lett.* **16**, 1955–1957 (1991)
- J.J. Zayhowski, Q-switched operation of microchip lasers. *Opt. Lett.* **16**, 575 (1991)
- J.J. Zayhowski, C. Dill III, Diode-pumped passively Q-switched picosecond microchip lasers. *Opt. Lett.* **19**, 1427 (1994)
- J.J. Zayhowski, Microchip lasers. *Opt. Mater.* **11**, 255–267 (1999)
- J.J. Zayhowski, Passively Q-switched Nd:YAG microchip lasers and applications. *J. Alloy. Compd.* **303–304**, 393–400 (2000)
- F. Liu, J. He, B. Zhang, J. Xu, X. Dong, K. Yang, H. Xia, H. Zhang, Diode-pumped passively Q-switched Nd:LuVO₄ laser at 1.34 μm with a V³⁺:YAG saturable absorber. *Opt. Express* **16**, 11759–11763 (2008)
- J. Šulc, J. Novák, H. Jelínková, K. Nejezchleb, V. Škoda, 1444-nm Q-switched pulse generator based on Nd:YAG/V:YAG microchip laser. *Laser Phys.* **20**, 1288–1294 (2010)
- R. Fluck, B. Braun, E. Gini, H. Melchior, U. Keller, Passively Q-switched 1.34 μm Nd:YVO₄ microchip laser with semiconductor saturable-absorber mirrors. *Opt. Lett.* **22**, 991–993 (1997)
- R. Häring, R. Paschotta, R. Fluck, E. Gini, H. Melchior, U. Keller, Passively Q-switched microchip laser at 1.5 μm . *J. Opt. Soc. Am. B* **18**, 1805–1812 (2001)
- G.J. Spühler, R. Paschotta, M.P. Kullberg, M. Graf, M. Moser, E. Mix, G. Huber, C. Harder, U. Keller, A passively Q-switched Yb:YAG microchip laser. *Appl. Phys. B Lasers Opt.* **72**, 285–287 (2001)
- D. Nodop, J. Limpert, R. Hohmuth, W. Richter, M. Guina, A. Tünnermann, High-pulse-energy passively Q-switched quasi-monolithic microchip lasers operating in the sub-100-ps pulse regime. *Opt. Lett.* **32**, 2115–2117 (2007)
- A. Steinmetz, D. Nodop, A. Martin, J. Limpert, A. Tünnermann, Reduction of timing jitter in passively Q-switched microchip lasers using self-injection seeding. *Opt. Lett.* **35**, 2885–2887 (2010)
- E.R. Thoen, E.M. Koontz, M. Joschko, P. Langlois, T.R. Schibli, F.X. Kärtner, E.P. Ippen, L.A. Kolodziejski, Two-photon absorption in semiconductor saturable absorber mirrors. *Appl. Phys. Lett.* **74**, 3927–3929 (1999)
- M. Haiml, R. Grange, U. Keller, Optical characterization of semiconductor saturable absorbers. *Appl. Phys. B Lasers Opt.* **79**, 331–339 (2004)
- R. Grange, M. Haiml, R. Paschotta, G.J. Spühler, L. Krainer, M. Golling, O. Ostinelli, U. Keller, New regime of inverse saturable absorption for self-stabilizing passively mode-locked lasers. *Appl. Phys. B Lasers Opt.* **80**, 151–158 (2005)
- W. Koechner, in *Springer Series in Optical Sciences*, 5th edn., ed. by A.L. Schawlow, T. Tamir, A. E. Siegman. Solid-State Laser Engineering, Chap. 8 (Springer, Berlin, 1999)
- W. Richter, BATOP GmbH, Jena (personal communication, 2009)
- A. Brignon, G. Feugnet, J.P. Huignard, J.P. Pocholle, Compact Nd:YAG and Nd:YVO₄ amplifiers end-pumped by a high-brightness stacked array. *IEEE J. Quantum Electron.* **34**, 577–585 (1998)
- J.J. Degnan, D.B. Coyle, R.B. Kay, Effects of thermalization on Q-switched laser properties. *IEEE J. Quantum Electron.* **34**, 887–899 (1998)

24. A.A. Demidovich, S.V. Voitkov, L.E. Batay, A.S. Grabtchikov, M.B. Danailov, V.A. Lisinetskii, A.N. Kuzmin, V.A. Orlovich, Modeling and experimental investigation of short pulse Raman microchip laser. *Opt. Commun.* **263**, 52–59 (2006)
25. O. Guillot-Noël, A. Kahn-Harari, B. Viana, D. Vivien, E. Antic-Fidancev, P. Porcher, Optical spectra and crystal field calculations of Nd³⁺ doped Zircon-type YMO₄ laser hosts (M = V, P, As). *J. Phys. Condens. Matter* **10**, 6491 (1998)
26. J. Zayhowski, in *Solid-State Lasers and Applications*, ed. by A. Sennaroglu. Passively Q-Switched Microchip Lasers, Chap. 1 (CRC Press, Boca Raton, 2006)
27. J.J. Zayhowski, J.A.L. Wilson, Energy-scavenging amplifiers for miniature solid-state lasers. *Opt. Lett.* **29**, 1218–1220 (2004)